A Subseasonal Teleconnection Analysis: PNA Development and Its Relationship to the NAO

STEPHEN BAXTER AND SUMANT NIGAM

University of Maryland, College Park, College Park, Maryland

(Manuscript received 12 July 2012, in final form 28 December 2012)

ABSTRACT

The Pacific–North American (PNA) teleconnection is a major mode of Northern Hemisphere wintertime climate variability, with well-known impacts on North American temperature and precipitation. To assess whether the PNA teleconnection has extended predictability, comprehensive data analysis is conducted to elucidate PNA evolution, with an emphasis on patterns of PNA development and decay. These patterns are identified using extended empirical orthogonal function (EEOF) and linear regression analyses on pentad-resolution atmospheric circulation data from the new Climate Forecast System Reanalysis (CFSR). Additionally, dynamical links between the PNA and another important mode of wintertime variability, the North Atlantic Oscillation (NAO), are analyzed both in the presence and absence of notable tropical convections, for example, the Madden–Julian oscillation (MJO), which is known to be influential on both. The relationship is analyzed using EEOF and regression techniques.

It is shown that the PNA structure is similar in both space and time when the MJO is linearly removed from the dataset. Furthermore, there is a small but significant lag between the NAO and PNA, with the NAO leading a PNA of opposite phase on time scales of one to three pentads. It is suggested from barotropic vorticity analysis that this relationship may result in part from excitation of Rossby waves by the NAO in the Asian waveguide.

1. Introduction

The Pacific–North American (PNA) teleconnection pattern is a major mode of Northern Hemispheric midlatitude climate variability (Wallace and Gutzler 1981). The well-known pattern consists of four centers of action with alternating signs: the subtropical northeastern Pacific, the Gulf of Alaska, northwestern North America, and the southeastern United States. The pattern has important implications for sensible hydroclimate variability, particularly during winter over North America. Better understanding of the development of PNA patterns can have a positive impact on intraseasonal climate prediction where current prediction is relatively weak. Currently, we are afforded reasonable forecast skill out to two weeks or so from traditionally numerical weather prediction. Longer-lead climate forecasts are made possible because of slowly varying boundary conditions (e.g., ENSO). However, the subseasonal time frame that exists between the two (weeks 3–5) remains a difficult problem. Being able to identify any nascent phase is potentially helpful in terms of being able to diagnose the climate state and therefore increase the ability to predict its evolution.

A recent study by Franzke et al. (2011) used composite analysis among other techniques to show that both phases of the PNA can be weakly excited by tropical convection before achieving its mature amplitude 8–12 days later. It is suggested there that tropical convection plays an essential role in the excitation of PNA events. Additionally, intraseasonal tropical convection related to the Madden–Julian oscillation (MJO; Madden and Julian 1971, 1972) has been shown to contribute to both PNA development (Higgins and Mo 1997) and the North Atlantic Oscillation (NAO; Lin et al. 2009). The aforementioned studies would suggest that weakened convection in the eastern Indian Ocean and enhanced convection in the western tropical Pacific [a high real-time multivariate MJO (RMM) 2 index] would lead to a positive PNA followed by a negative NAO. As we will show, the intraseasonal analysis bears out something quite different, with the NAO leading a PNA of opposite sign.

Corresponding author address: Stephen Baxter, Jull Hall 3118, University of Maryland, College Park, College Park, MD 20742.
E-mail: sbaxter@atmos.umd.edu

DOI: 10.1175/JCLI-D-12-00426.1

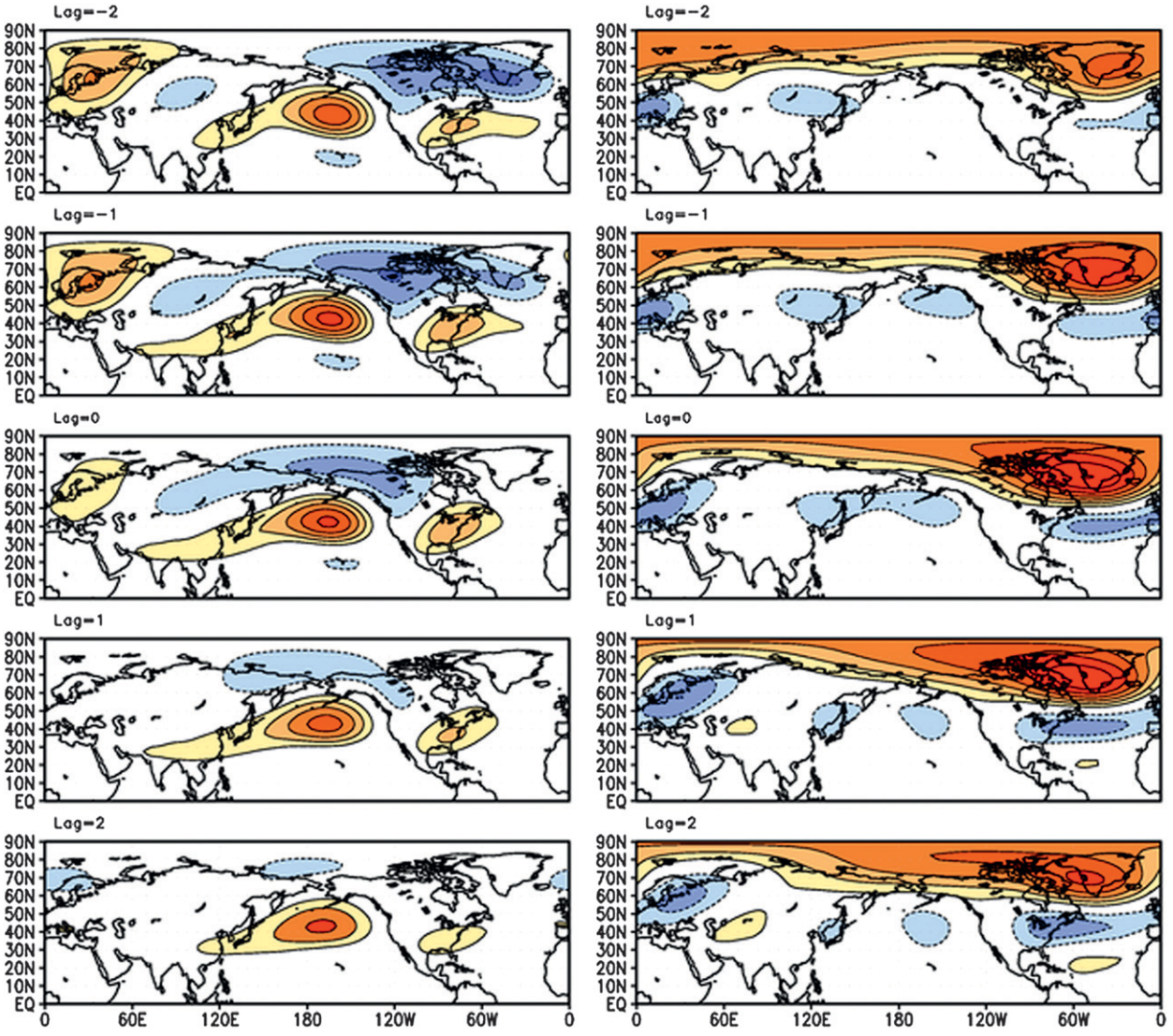

FIG. 1. (left) REEOF mode 4, constituting the PNA pattern. The pattern seems to reach maximum amplitude at lags 0 and −1. Contour interval is 20 m. (right) REEOF mode 1, constituting the NAO pattern. This pattern peaks at lags 0 and 1. Contour interval is 20 m.

This study uses empirical orthogonal function (EOF) analysis to identify teleconnection patterns, with particular emphasis on the PNA, and assesses how that might be sensitive to the MJO. The data and methods used are detailed in section 2. Additionally, we assess the lagged relationship between the PNA and NAO and seek some physical explanation for the observed results. These are detailed in section 3. A brief discussion of results follows in section 4.

2. Data and methods

We employ the state-of-the-art Climate Forecast System Reanalysis (CFSR; Saha et al. 2010) for rotated extended empirical orthogonal function (REEOF) analysis on Northern Hemispheric extended wintertime (November–March, 1979–2008) 200-mb height anomalies at pentad resolution that have been latitudinally weighted. The extended EOF analysis, in contrast with traditional EOF analysis, produces loading vectors that consist of a five-pentad series of spatial patterns associated with a single principal component time series. This allows us to potentially elucidate nascent teleconnection phases as they actually appear in the data, rather than their statistical representation in lead–lag regressions. While many teleconnection analyses are conducted at the 500-mb level, we use the 200-mb level since we are interested in the potential interaction between the tropics and the midlatitudes. The equivalent barotropic nature of the teleconnections that emerges when any method of

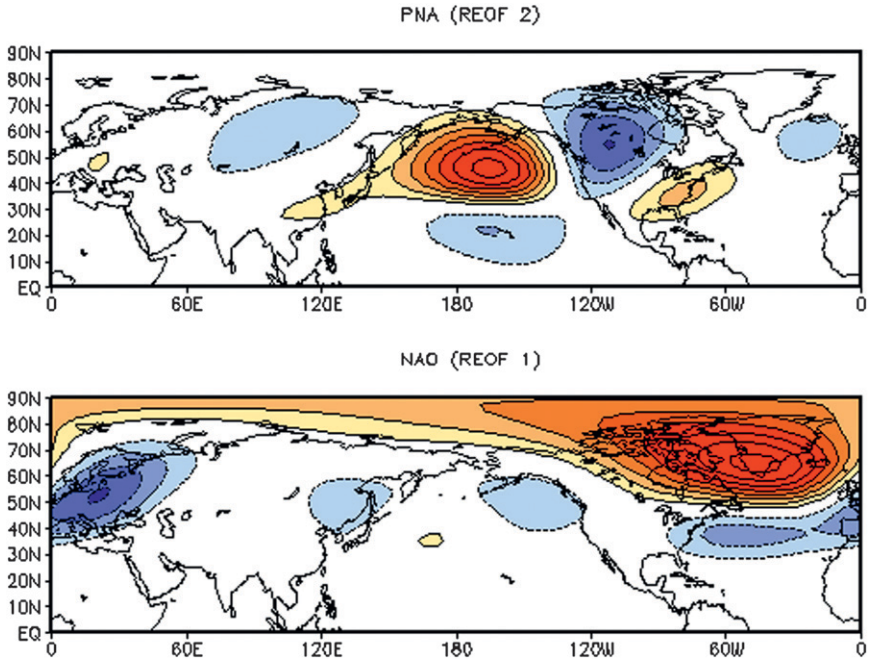

FIG. 2. The two leading modes that emerge from the REOF analysis constitute the (top) PNA and (bottom) NAO. Contour interval is 20 m.

removing daily fluctuations is used allows us to utilize 200 mb without loss of the essential centers of action. The analysis is conducted using the covariance matrix and the seven leading modes are rotated using the varimax criterion (Barnston and Livezy 1987) to allow for more spatial discrimination.

The analysis is repeated, this time using data from which the MJO is linearly removed by subtracting the contemporaneous regressions of the Wheeler and Hendon RMM 1 and RMM 2. These indices were created from the CFSR using the method established by Wheeler and Hendon (2004) to capture the propagating nature of MJO-related convection. The RMM 1 regression onto outgoing longwave radiation (OLR) reveals a convective heating source over the Maritime Continent; RMM 2 captures a dipole between the Indian Ocean and west Pacific.

Rotated nonextended EOF analysis (REOF) is also conducted to compare with the REEOF analysis with the goal of being able to assess the value that extended EOF analysis adds to the study. A series of lead–lag regressions are then performed.

To understand the physical connection between the NAO and PNA, we look at simple terms in the barotropic vorticity equation, namely, the beta term that accounts for advection of planetary vorticity and the orographic forcing term. Each is assessed using the NAO's principal component (from the REEOF) regression onto the different wind fields used in each term.

3. Results

The REEOF analysis pulls out the most frequently occurring five-pentad series of 200-mb height anomaly patterns. In this framework, the NAO emerges as the leading mode (Fig. 1), explaining 6.7% of the total variance. The PNA pattern emerges as the fourth-leading mode (Fig. 1), explaining 4.6% of the variance. The modes are displayed as the regression of the normalized principal components (PCs) onto the height field. The seemingly small percentage of explained variance is due to the nature of the extended analysis, since in the place of each spatial pattern in the covariance matrix, a five-pentad series of patterns is used, increasing the total variance. Note that the figures shown here constitute the negative phase of the traditional teleconnection definitions. This polarity difference is unimportant. The second- and third-leading modes (not shown) may be associated with separate development and decaying phases of a mode similar to the North Pacific Oscillation, something that warrants further analysis.

Figure 1 yields two interesting results: 1) the maximum amplitude of the PNA mode appears closer to $T-1$ (T is used for the time sequence of spatial patterns, while t will be used to refer to the time series itself), so the mode is focusing slightly more on the decaying phase of the PNA, and 2) there is an NAO-type anomaly of opposite sign preceding the PNA that exhibits noticeable

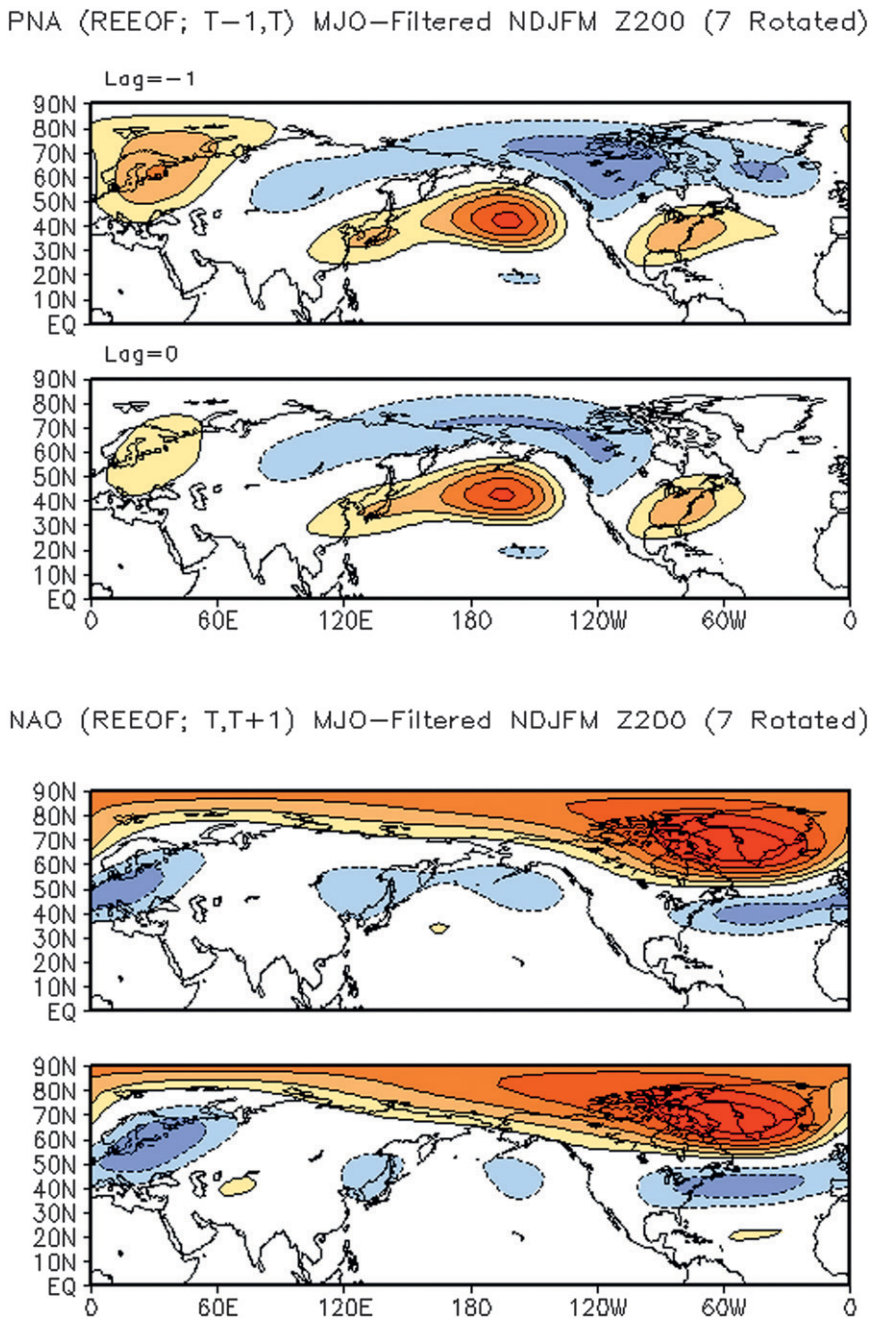

FIG. 3. The maximum amplitudes that emerge from REEOF analysis with MJO-filtered data for the (top) PNA and (bottom) NAO patterns. Contour interval is 20 m.

westward propagation through the sequence. A similarly interesting result from Fig. 1 shows that the NAO pattern seems to peak nearer to $T + 1$. Therefore, both loading vectors are asymmetric about $T = 0$. In this way, the purely statistical analysis could be revealing something very physical about the underlying system, namely, that the development and decay of the PNA and NAO may be related on subseasonal time scales. Because matrix algebra constrains the principal components to be temporally independent, shifting the series of spatial patterns within the loading vector must compensate for any robust physical connection between the two modes.

From the nonextended REOF analysis, the NAO and PNA emerge as modes 1 and 2, explaining 10.4% and

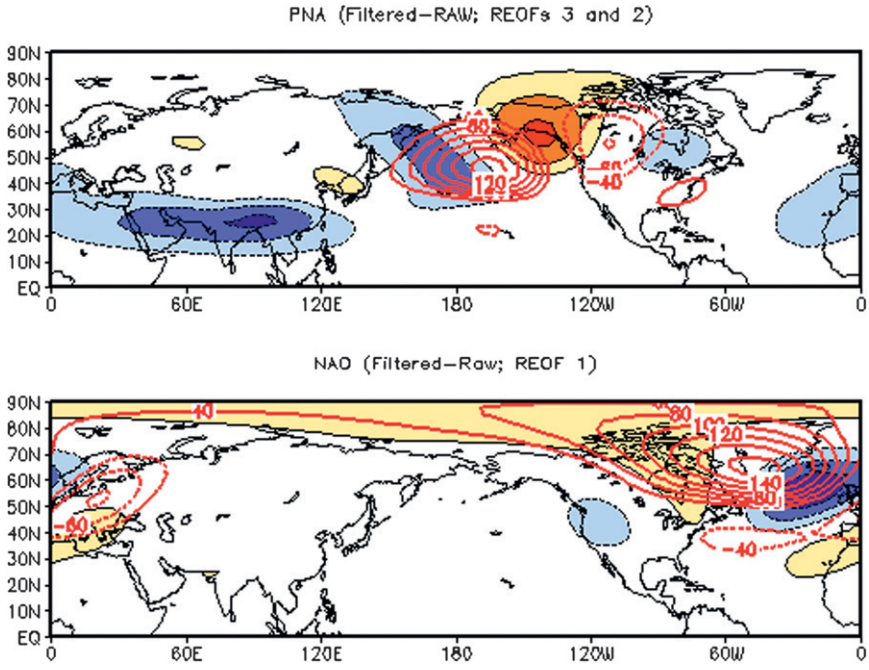

FIG. 4. Red contours show mature (top) PNA and (bottom) NAO from REOF analysis; shading is the difference between MJO-filtered and nonfiltered analysis. Contour interval is 3 m.

7.8% of the variance, respectively (Fig. 2). There is a sizable difference between the patterns that emerge from the REEOF analysis and the lead–lag regressions associated with the nonextended analysis. This is consistent with analysis of Nigam (2003), which used weekly lead–lag regressions from a nonextended analysis to assess evolution of the PNA pattern. This difference highlights the importance and relative novelty of using REEOF analysis in subseasonal teleconnection studies.

Sensitivity to the number of modes rotated in the analysis was tested using the nonextended REOF. The PNA pattern emerges as a leading pattern, explaining roughly the same percentage of variance whether 4, 10, or the chosen 7 modes are rotated (not shown). This is expected given that the two leading patterns (NAO and PNA) are not as likely to be as sensitive to the number of rotated modes as would be subsequent modes in the analysis.

Next, we assess how linear removal of two orthogonal MJO principal components affects both the REOF analysis and the REEOF analysis. The PNA and NAO emerge as leading modes at fourth and first, respectively, in the REEOF analysis; this is the same as in the original analysis. In the nonextended analysis, however, MJO filtering results in the PNA falling from the second- to the third-leading mode of variability. Figure 3 shows the PNA and NAO in their respective mature phases in the REEOF analysis when the MJO has been removed. These figures are nearly identical to those that fall out of the original analysis. There is no noticeable shift in space or time of the essential centers of action. The only visually identifiable change in the PNA pattern occurs over south-central and Southeast Asia, which makes sense since that is where the MJO has a very strong footprint in the geopotential height field (not shown).

Closer inspection, however, reveals that the MJO removal results in a very modest shift (an order of magnitude weaker) in the centers of action of both the PNA and the NAO. Figure 4 shows the difference between the original and MJO-filtered analysis from the nonextended analysis. The differences are plotted in the context of the original mature patterns. The mid- and high-latitude PNA centers are generally shifted east, while the NAO centers of action are shifted northwest. In the PNA case, the differences appear visually as a wave train emanating from the MJO source region.

As previously mentioned, the evolution of the PNA pattern reveals an NAO-type pattern of opposite sign that precedes the mature PNA. The lag correlation between the PNA mode and the NAO mode is shown in Fig. 5; results from the original and MJO-filtered REEOF analyses are both plotted, as are results from the REOF and station-based analyses. The lag correlation is greatest in the REEOF analysis, with a positive PNA

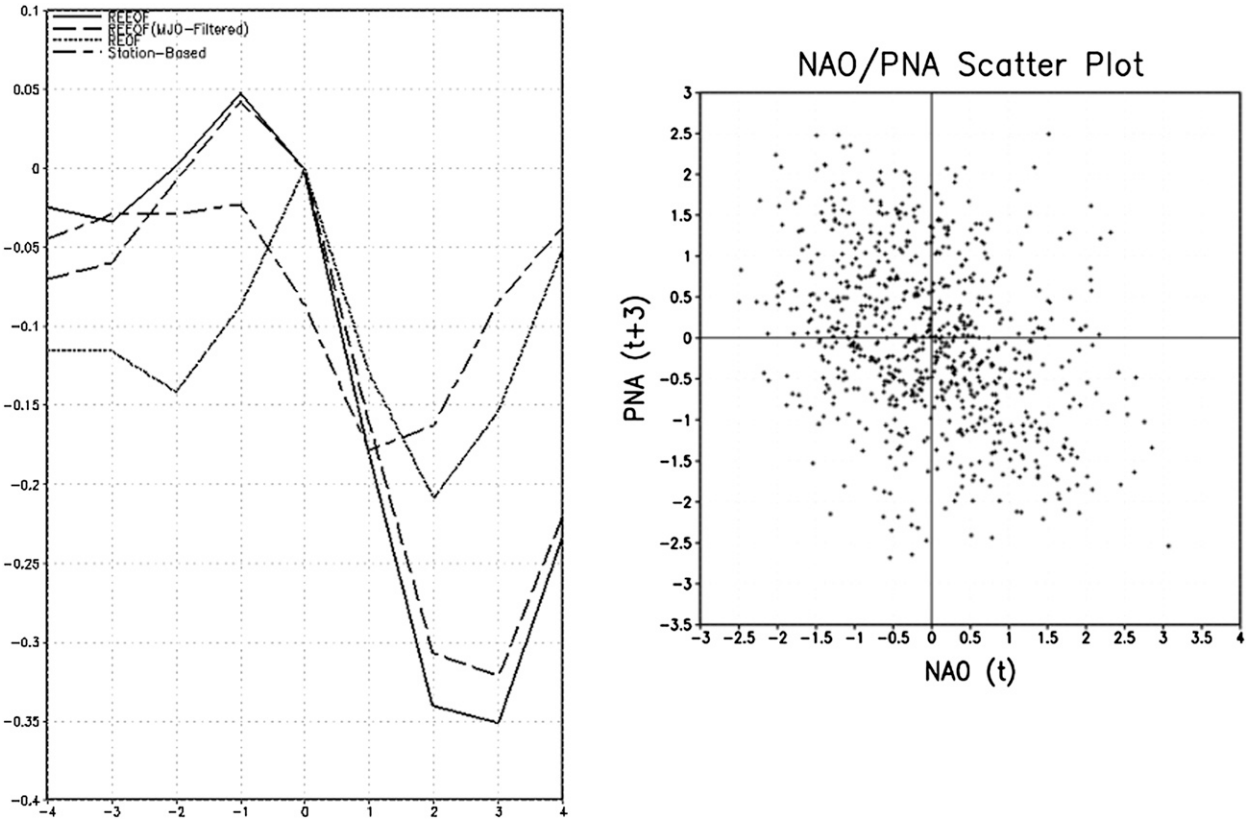

FIG. 5. (left) Correlation between the NAO and PNA indices as defined by REEOF analysis, REEOF analysis from which the MJO was linearly removed, REOF analysis, and a station-based analysis at 500 mb. Correlation coefficients are a function of lagged pentads. Positive lag corresponds to PNA lagging the NAO. (right) Scatterplot of principal component is shown for PNA at time $t + 3$ and NAO at time t emerging from REEOF analysis. There is noticeable clustering in the negative quadrants.

lagging a negative NAO by two or three pentads and vice versa. The magnitude of the lag may be exaggerated in the REEOF analysis since the NAO mode peaks near $T + 1$ and the PNA appears to peak prior to $T = 0$. Additionally, the REEOF PCs vary more slowly, lending themselves to higher lag correlations and thus reducing degrees of freedom. That being said, the REOF analysis reveals the same qualitative result (Fig. 5), and the peak amplitudes are statistically significant beyond a 99% confidence limit. A similar analysis using station-based NAO and PNA indices (Fig. 5) reveals the same lag at one to two pentads, also lending further support to our methodology.

A more aesthetically satisfying portrayal of this lag between the NAO and a PNA of opposite phase is also seen in Fig. 5. That scatterplot reveals an anticipated negative slope between the NAO at time t and the PNA at time $t + 3$. The clear clustering in the negative quadrants shows that this relationship is not an artificial product of outliers. Furthermore, the presence of some apparent outliers in the first quadrant suggests the relationship may be more robust than the correlation coefficients themselves reveal.

While this intraseasonal relationship between the NAO and the PNA is both novel and robust by itself, we must be interested in positing some physical explanation for the observed interaction. With that goal in mind, simple terms in the barotropic vorticity equation are evaluated with respect to the NAO:

$$\frac{\partial \zeta}{\partial t} = -\beta v^{\mathrm{NAO}}_{200\,\mathrm{mb}} - \frac{f}{H}(\mathbf{V}^{\mathrm{NAO}}_{850\,\mathrm{mb}} \cdot \nabla h) - (\mathbf{V}^{\mathrm{NAO}}_{200\,\mathrm{mb}} \cdot \nabla \zeta \mathrm{clim}),$$

where ζ is the relative vorticity at 200 mb and β is the meridional derivative of the Coriolis parameter f. The meridional wind is given by v, and $\mathbf{V}$ is the vector wind. The topography h is used, as is H, which is the height of the troposphere, assumed here to be a constant 10 km. Superscript NAO means this is the regression coefficient of the REEOF PC that constitutes the NAO onto the wind at a level given by the subscript. The term on the left-hand side is the local tendency term. The right-hand

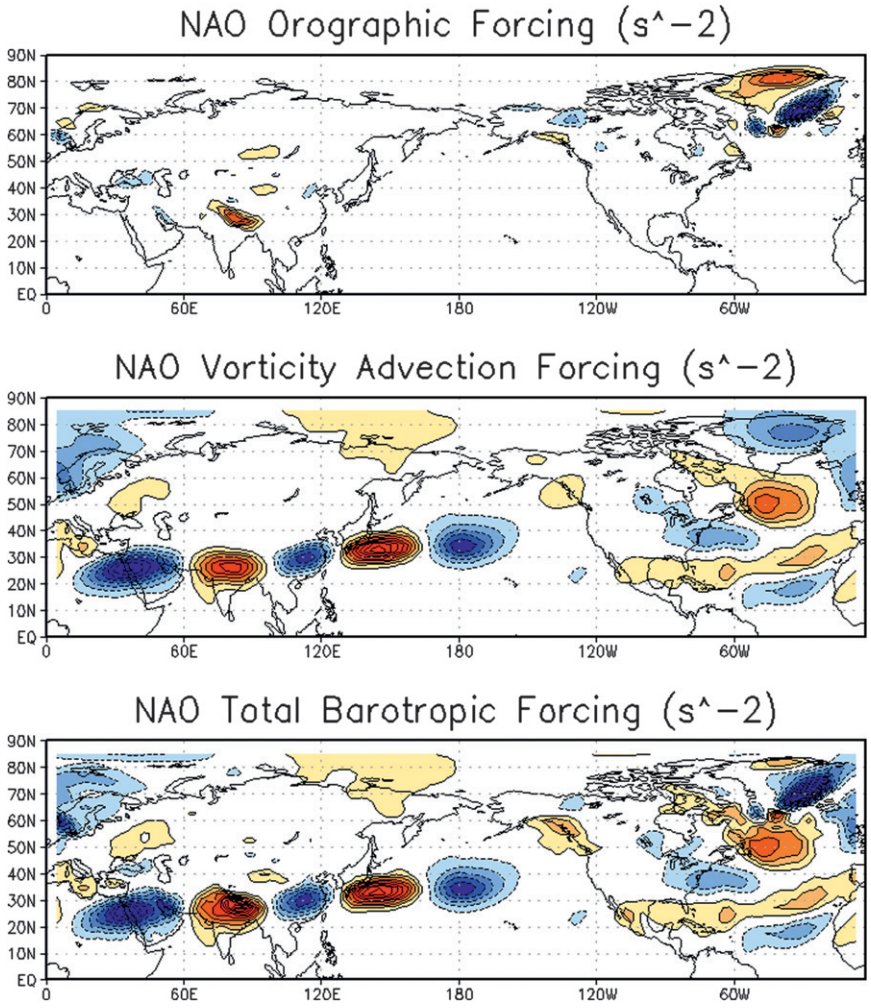

FIG. 6. Three terms in the barotropic vorticity equation are evaluated with respect to the NAO regression on the respective circulation fields: (top) orographic forcing, (middle) the sum of the beta term and advection of the climatological relative vorticity, and (bottom) the sum of all three. The contour interval is $10^{-11}\,s^{-2}$. Each panel shows the contribution of that term to negative vorticity tendency ($-\partial\zeta/\partial t$), so the warm colors are proportional to positive height tendency.

side consists of the beta term, the divergence term, and the relative vorticity advection term. The outstanding question is whether the NAO can force the PNA via retrogression of mid- and high-latitude anomalies, rapid downstream energy propagation, or both. The terms analyzed are the beta term, which consists of beta multiplied by the NAO regression onto the meridional wind at 200 hPa; the orographic forcing term (divergence term), which is calculated as the dot product between the NAO regression onto the 850-hPa wind field and the gradient of topography; and the advection of climatological relative vorticity by the NAO regression onto the 200-hPa wind. We can safely neglect any relative vorticity advection because of the concentric, symmetric nature of the teleconnection footprints. Figure 6 shows the total advection and orographic terms as well as their sum. This sum constitutes the opposite of local relative vorticity tendency ($-\partial\zeta/\partial t$), which is proportional to geopotential height tendency. The analysis is particularly revealing because the use of beta allows for a more tropical signature while the meridional wind allows for a better sense of wave propagation. The regression of the teleconnections onto the zonal wind is certainly of much larger magnitude than the regression onto the meridional wind, but it is in fact the meridional wind that may be more important because of its inclusion in the beta term.

Figure 6 reveals that the NAO indeed forces a wave pattern that starts in the northern tropics near the zonal jet maximum that is climatologically present near the Arabian Peninsula. This pattern seems to terminate at the end of the East Asian jet stream, which coincides with the semipermanent Aleutian low, a main center of action of the PNA. At the same time, the beta term supports a retrogression of NAO anomalies westward across northern North America. Additionally, the orographic term strongly supports the beta forcing in two key areas: south-central Asia (Himalayas) and the Alaskan panhandle.

4. Discussion

The PNA emerges as a leading pattern of variability from REEOF analysis of 29 extended winter seasons at pentad resolution with an interesting lagged connection to the NAO, with the NAO leading a PNA pattern of the opposite sign. The REEOF PNA pattern shows a peak closer to time $T - 1$, while the NAO pattern from the same analysis peaks closer to $T + 1$. Given that the two modes in this analysis are statistically constrained to be temporally independent, this may highlight an intrinsic and physical connection between the two on intraseasonal time scales. The manifestation of this connection on subseasonal time scales is particularly interesting given that historically little attention is paid to the identification of teleconnections at this temporal resolution. It is our belief that further understanding the physical basis of this relationship will aid in efforts to predict climate variability in this time frame, which is of growing importance.

When the analysis is repeated on the data from which the MJO has been linearly removed, there is little visually noticeable difference. In fact, the only small differences appear as subtle shifts in the modes' centers of action. The fact that MJO removal has little or no impact reveals two points, both of which are likely valid: 1) nonlinear and lagged impacts of the MJO cannot be removed and thus the MJO is still contributing in a small way and 2) while MJO or related intraseasonal tropical convection trigger PNA events, the PNA is likely a mode of variability intrinsic to the midlatitude atmosphere, occurring even in the absence of canonical MJO-related tropical convection. It has been noted by other studies (e.g., Lin and Brunet 2009; Lin et al. 2010) that the MJO impacts North America via a Rossby wave train that is instigated by an MJO-induced convective dipole between the eastern Indian Ocean and the western Pacific Ocean. These MJO impacts therefore necessarily exist at some lag. It is therefore likely that even linear impacts of the MJO on the PNA and especially the NAO are not being removed because they exist at some lag (~3 pentads in the case of the NAO, less for PNA). This would not be a problem by itself since, in a perfectly propagating MJO, lagged impacts from RMM 2 manifest themselves as contemporaneous impacts from RMM 1. However, not all MJO events are ideal, and thus, it is likely that the MJO removal is far from perfect. Additionally, contribution from other subseasonal tropical convective signals (e.g., atmospheric Kelvin waves and equatorial Rossby waves) cannot be precluded. Again, the key finding here is that MJO is not essential for the existence of the PNA.

As mentioned previously, it is important to advance a hypothesis on the physical basis for the connection between the NAO and the PNA. The brief analysis of the simple barotropic vorticity equation indeed gives some indication of how the NAO may be forcing the PNA. The total advection term shows the vorticity forcing from the NAO results in both westward propagation of the longwave pattern across North America and in energy propagation to the Arabian Peninsula and through southern and eastern Asia, culminating in the Pacific. This is remarkably consistent with the results of Hoskins and Ambrizzi (1993), which found preferred propagation from Europe to the Arabian Peninsula. Additionally, they showed how the East Asian jet stream serves as a Rossby waveguide. It is in this light that we suggest the NAO excites a wave train in the vicinity of the Arabian Sea that ultimately forces a PNA pattern of opposite sign. This in combination with westward propagation of high-latitude NAO anomalies that accounts for the observed connection between the NAO and the PNA.

REFERENCES

Barnston, A., and R. Livezy, 1987: Classification, seasonality, and persistence of low-frequency atmospheric circulation patterns. *Mon. Wea. Rev.,* **115,** 1083–1126.

Franzke, C., S. Feldstein, and S. Lee, 2011: Synoptic analysis of the Pacific–North American teleconnection pattern. *Quart. J. Roy. Meteor. Soc.,* **137,** 329–436.

Higgins, R., and K. Mo, 1997: Persistent North Pacific circulation anomalies and the tropical intraseasonal circulation. *J. Climate,* **10,** 223–244.

Hoskins, B. J., and T. Ambrizzi, 1993: Rossby wave propagation on a realistic longitudinally varying flow. *J. Atmos. Sci.,* **50,** 1661–1671.

Lin, H., and G. Brunet, 2009: The influence of the Madden–Julian oscillation on Canadian wintertime surface air temperature. *Mon. Wea. Rev.,* **137,** 2250–2262.

——, ——, and J. Derome, 2009: An observed connection between the North Atlantic Oscillation and the Madden–Julian oscillation. *J. Climate,* **22,** 364–380.

——, ——, and R. Mo, 2010: Impact of the Madden–Julian oscillation on wintertime precipitation in Canada. *Mon. Wea. Rev.,* **138,** 3822–3839.

Madden, R., and P. Julian, 1971: Detection of a 40–50 day oscillation in the zonal wind in the tropical Pacific. *J. Atmos. Sci.,* **28,** 702–708.

——, and ——, 1972: Description of global-scale circulation cells in the tropics with a 40–50 day period. *J. Atmos. Sci.,* **29,** 1109–1123.

Nigam, S., 2003: Teleconnections. *Encyclopedia of Atmospheric Sciences,* J. R. Holton, J. A. Pyle, and J. A. Curry, Eds., Academic Press, 2243–2269.

Saha, S., and Coauthors, 2010: The NCEP Climate Forecast System Reanalysis. *Bull. Amer. Meteor. Soc.,* **91,** 1015–1057.

Wallace, J., and D. Gutzler, 1981: Teleconnections in the geopotential height field during the Northern Hemisphere winter. *Mon. Wea. Rev.,* **109,** 784–804.

Wheeler, M. C., and H. H. Hendon, 2004: An all-season real-time multivariate MJO index: Development of an index for monitoring and prediction. *Mon. Wea. Rev.,* **132,** 1917–1932.